Compact Microstrip BPF with High Selectivity Using Extended Tapped Lines

Yi-Qiang Gao[1, 2], Wei Shen[3], Liang Wu[1], and Xiao-Wei Sun[1, *]

Abstract—This paper proposes a compact microstrip bandpass filter (BPF) with high selectivity. A folded stepped-impedance resonator (SIR) of which the high impedance part is realized by a coplanar waveguide on the ground layer is introduced to the filter design for miniaturization. Furthermore, source-load coupling is implemented by extended tapped lines (ETLs). High selectivity with four transmission zeros (TZs) can be achieved. The analysis of the filter is presented based on a transmission line circuit model and even- and odd-mode analysis method. An experimental filter with the size of $0.15\lambda_g * 0.13\lambda_g$ (where λ_g is the guide wave-length at the center frequency) is designed to validate our methods.

1. INTRODUCTION

With the increasing tension of spectrum resources, highly selective filters have become an important part of the front-ends. Bandpass filters (BPFs) can be an effective choice to obtain the required signal to noise ratio. Various techniques have been introduced to achieve transmission zeros (TZs) to realize high selectivity. Cross-coupling and source-load coupling are used simultaneously in a fourth-order waveguide BPF to achieve four near band TZs [1]. Stepped-impedance resonators with mixed cross-coupling are proposed to achieve one more TZ [2]. In addition, source-load coupling is also an easy way to accomplish better selectivity. A large number of studies have used sourceload coupling to achieve transmission zeros (TZs) near the passband and realize high selectivity [3–9]. Four shorted quarter-wavelength coplanar waveguide (CPW) resonators as well as shorted CPW excitation lines are introduced to realize capacitive crosscoupling and inductive source-load coupling respectively [3]. The filter with better frequency skirt is achieved with six TZs. However, the implementation is complicated as bonding wires are needed to keep common ground. A dual mode resonator with capacitive and inductive source-load coupling is analyzed in [4, 5], respectively. But only one TZ can be placed really near the passband. A simple and effective second-order BPF with a TZ on each side of the passband is realized by parallel coupled quarter-wavelength resonators and inductive source-load coupling [6]. Mixed source-load coupling is adopted in the substrate integrated waveguide (SIW) [7, 8] and microstrip filters [9]; three TZs can be obtained. In general, however, the dimensions of SIW filters can be larger than the microstrip ones in low frequency.

In this paper, a compact BPF with high selectivity is designed using a novel source-load coupling structure. Extended tapped lines (ETLs) implemented at the I/O ports are used to excite the resonators as well as realize source-load coupling. Three TZs near the passband are obtained to improve frequency selectivity, and one TZ at high stopband is used to suppress a harmonic passband. Besides, a folded SIR is used to achieve miniaturization, of which the high impedance section is realized by CPW on the ground plane. In addition, transmission line circuit model as well as odd- and even-mode theory

analysis are presented. Then, full-wave simulation and measured results are demonstrated to verify the design methods, and the measured results agree with the simulated ones well.

2. FILTER CONFIGURATION AND ANALYSIS

As shown in Fig. 1(a), the proposed filter consists of three parallel coupled shorted quarter-wavelength SIRs (Z_1, Z_{2b}) (Z_3, Z_{2a}). To achieve a larger coupling coefficient, three SIRs are arranged in the interdigital form. ETLs (Z_4) are used to excite resonator 1 (R1) and resonator 3 (R3), also a part of the ETLs are coupled (Z_{e2}, Z_{o2}) to realize source-load coupling conveniently. According to [10], the three parallel coupled lines in dashed line frame can be transformed to two pairs of coupled lines (Z_{e1}, Z_{o1}) with the center SIR separated to middle connected two SIRs illustrated in dashed line frame of Fig. 1(b).
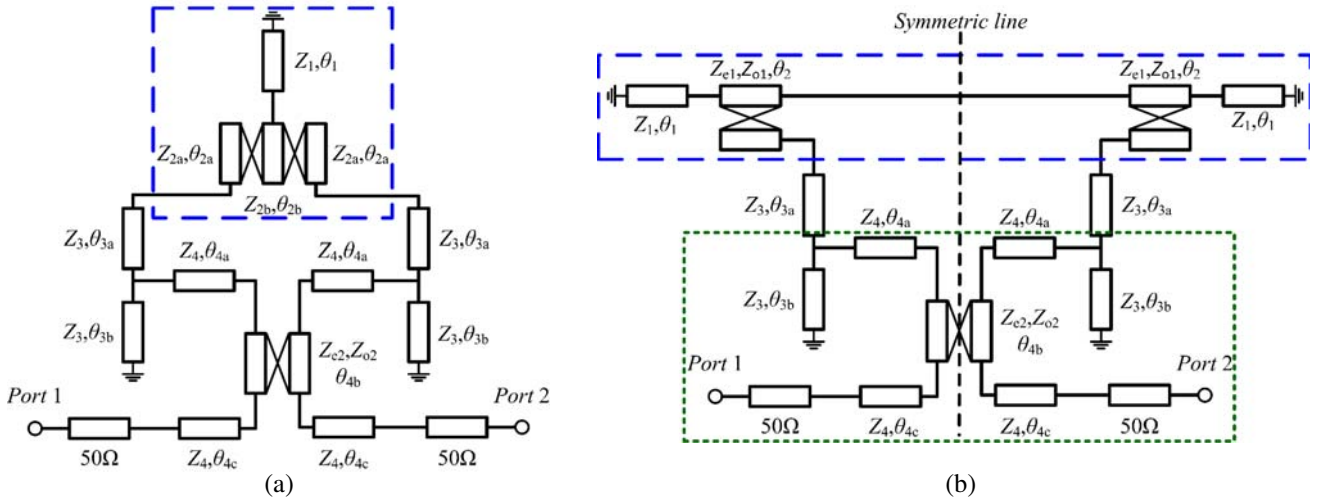

Figure 1. (a) Ideal transmission line circuit and (b) equivalent transmission line circuit of the proposed BPF.
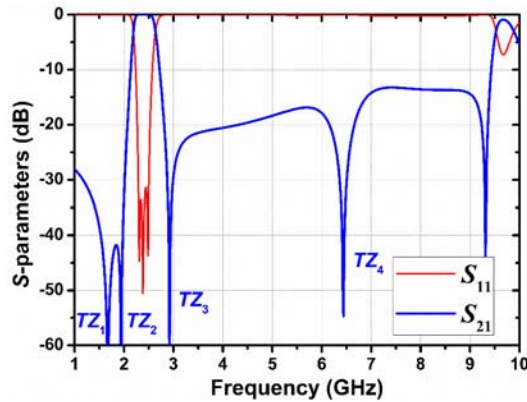
Figure 2. The calculated results of the equivalent transmission line circuit shown in Fig. 1(b) ($Z_1 = 90\,\Omega$, $Z_{o1} = 32\,\Omega$, $Z_{e1} = 49\,\Omega$, $Z_3 = 94\,\Omega$, $Z_4 = 115\,\Omega$, $Z_{o2} = 79\,\Omega$, $Z_{e2} = 144.5\,\Omega$, $\theta_1 = 37.6\,\text{deg}$, $\theta_2 = 30\,\text{deg}$, $\theta_{3a} = 5\,\text{deg}$, $\theta_{3b} = 37.3\,\text{deg}$, $\theta_{4a} = 5\,\text{deg}$, $\theta_{4b} = 16\,\text{deg}$, $\theta_{4c} = 42\,\text{deg}$).

The calculated results of the circuits in Fig. 1 are plotted in Fig. 2. The electric lengths of the transmission lines of Fig. 2 are calculated at the center frequency $f_0 = 2.4\,\text{GHz}$. Four TZs can be observed. Two TZs are at the lower stopband and one TZ is at the higher stopband near the passband, the other one are located at a higher stopband far away from the passband. Based on the symmetric
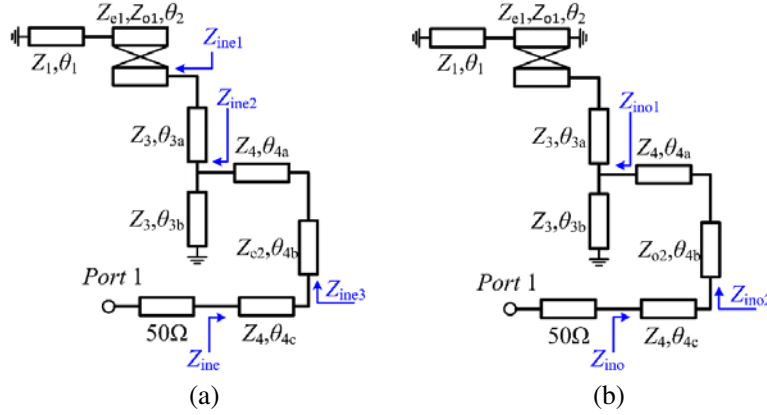
Figure 3. (a) Even-mode equivalent circuit. (b) Odd-mode equivalent circuit.

property of the circuit, the frequency responses can be derived by the odd- and even-mode analysis method [11]. The reflection response S_{11} and transmission response S_{21} are:

$$S_{11} = \frac{(Y_0^2 - Y_{ine}Y_{ino})}{(Y_0 + Y_{ine})(Y_0 + Y_{ino})} \tag{1}$$

$$S_{21} = \frac{Y_0(Y_{ino} - Y_{ine})}{(Y_0 + Y_{ino})(Y_0 + Y_{ine})} \tag{2}$$

The even- and odd-mode circuits are illustrated in Figs. 3(a) and 3(b), respectively. The input impedance Z_{ino1} is

$$Z_{ino1} = \frac{j(2TZ_3 \tan\theta_{3b} \cot\theta_2 - Z_3^2 \tan\theta_{3a} \tan\theta_{3b})}{2T(1 - \tan\theta_{3a} \tan\theta_{3b}) \cot\theta_2 - Z_3(\tan\theta_{3a} + \tan\theta_{3b})} \tag{3a}$$

where

$$T = \frac{Z_{e1}Z_{o1}}{Z_{e1} + Z_{o1}} \tag{3b}$$

and input impedance Z_{ino2} is

$$Z_{ino2} = \frac{Z_{o2}[Z_{ino1}(Z_4 - Z_{o2} \tan\theta_{4a} \tan\theta_{4b}) + jZ_4(Z_4 \tan\theta_{4a} + Z_{o2} \tan\theta_{4b})]}{Z_4(Z_{o2} - Z_4 \tan\theta_{4a}) \tan\theta_{4b} + jZ_{ino1}(Z_4 \tan\theta_{4b} + \tan\theta_{4a})} \tag{4}$$

Based on Equations (3)–(4) the input admittance of the odd-mode (Y_{ino}) can be derived as

$$Y_{ino} = \frac{Z_4 + jZ_{ino2} \tan\theta_{4c}}{Z_4 Z_{ino2} + jZ_4^2 \tan\theta_{4c}} \tag{5}$$

For the even-mode circuit in Fig. 3(b), the input impedance is

$$Z_{ine1} = \frac{A(j2Z_1 \tan\theta_1) + B}{C(j2Z_1 \tan\theta_1) + A} \tag{6}$$

where

$$A = (Z_{e1} + Z_{o1})/[(Z_{e1} - Z_{o1}) \cos\theta_1] \tag{7a}$$

$$B = j\frac{(Z_{e1} - Z_{o1})^2 - (Z_{e1} + Z_{o1})^2 \cos^2\theta_1}{2(Z_{e1} - Z_{o1}) \sin\theta_1} \tag{7b}$$

$$C = 2\sin\theta_1/(Z_{e1} - Z_{o1}) \tag{7c}$$

The input impedance Z_{ine2} and Z_{ine3} are

$$Z_{ine2} = \frac{-Z_3^2 \tan\theta_{3a} \tan\theta_{3b} + jZ_3 Z_{ine1} \tan\theta_{3b}}{Z_{ine1}(1 - \tan\theta_{3a} \tan\theta_{3b}) + jZ_3(\tan\theta_{3a} + \tan\theta_{3b})} \tag{8}$$

$$Z_{ine3} = \frac{Z_{e2}\left[Z_{ine2}(Z_4 - Z_{e2}\tan\theta_{4a}\tan\theta_{4b}) + jZ_4\left(Z_4\tan\theta_{4a} + Z_{e2}\tan\theta_{4b}\right)\right]}{Z_4(Z_{e2} - Z_4\tan\theta_{4a})\tan\theta_{4b} + jZ_{ine2}(Z_4\tan\theta_{4b} + Z_{e2}\tan\theta_{4a})} \tag{9}$$

According to Equations (6)–(9), the input admittance of the even-mode (Y_{ine}) can be derived as

$$Y_{ine} = \frac{Z_4 + jZ_{ine3}\tan\theta_{4c}}{Z_4 Z_{ine3} + jZ_4^2\tan\theta_{4c}} \tag{10}$$

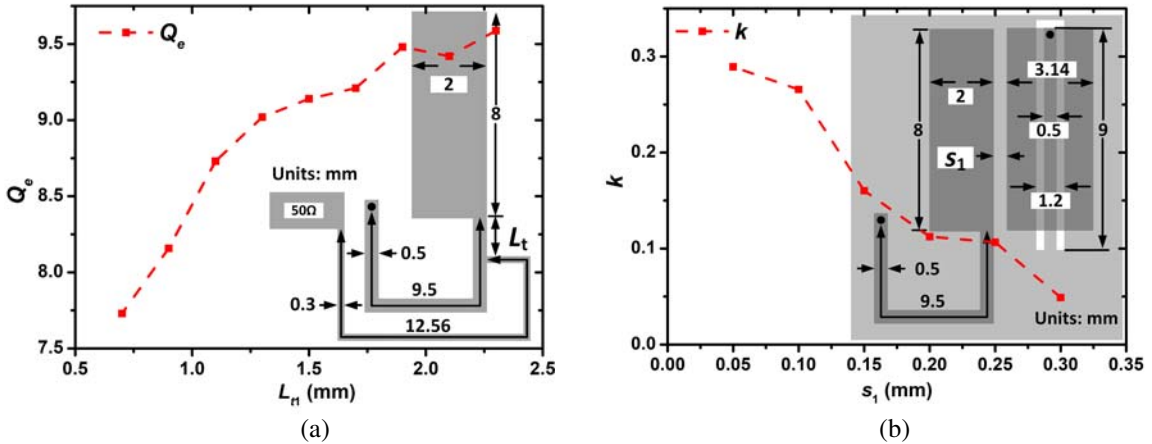Based on Equations (1)–(10), the functions of S-parameters depend on characteristic impedances, and electric lengths can be obtained easily.

2.1. Bandwidth and Port Excitation

The bandwidth of the proposed BPF is controlled by degree of the coupling among three parallel coupled SIRs. The bandwidths of the proposed BPF with different Z_{e1}, Z_{o1} and K_1 [$K_1 = (Z_{e1}Z_{o1})/(Z_{e1} + Z_{o1})$] are plotted in Fig. 4(a). For a larger K_1, the bandwidth of proposed BPF increases correspondingly. The

(a)   (b)
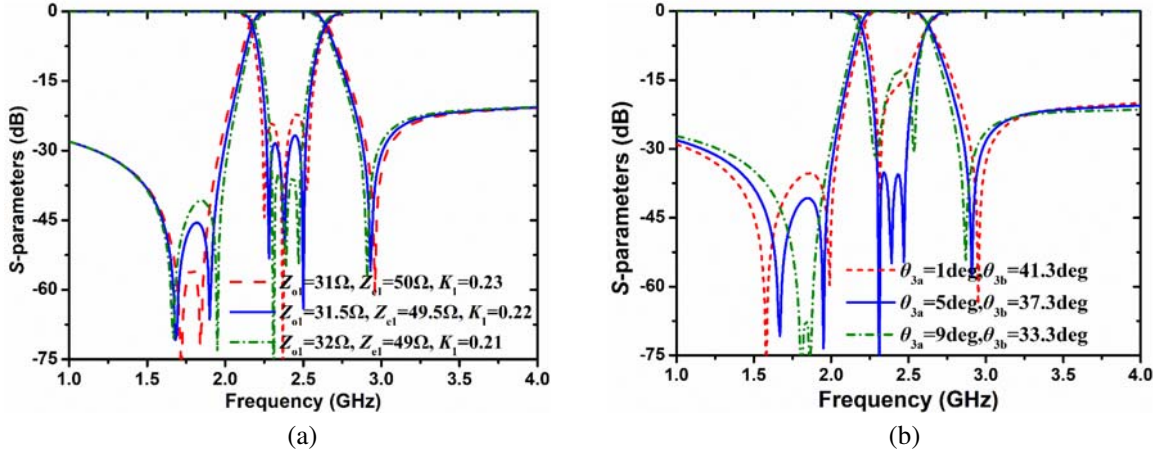
Figure 4. (a) Bandwidths of the proposed BPF with different Z_{e1}, Z_{o1} and K_1 [$K_1 = (Z_{e1} - Z_{o1})/(Z_{e1} + Z_{o1})$] ($Z_1 = 90\,\Omega$, $Z_3 = 94\,\Omega$, $Z_4 = 115\,\Omega$, $Z_{o2} = 79\,\Omega$, $Z_{e2} = 144.5\,\Omega$, $\theta_1 = 37.6\deg$, $\theta_2 = 30\deg$, $\theta_{3a} = 5\deg$, $\theta_{3b} = 37.3\deg$, $\theta_{4a} = 5\deg$, $\theta_{4b} = 16\deg$, $\theta_{4c} = 42\deg$) (b) frequency responses of the proposed BPF with different proportion of θ_{3a} in θ_3 ($\theta_3 = \theta_{3a} + \theta_{3b}$) ($Z_1 = 90\,\Omega$, $Z_{o1} = 32\,\Omega$, $Z_{e1} = 49\,\Omega$, $Z_3 = 94\,\Omega$, $Z_4 = 115\,\Omega$, $Z_{o2} = 79\,\Omega$, $Z_{e2} = 144.5\,\Omega$, $\theta_1 = 37.6\deg$, $\theta_2 = 30\deg$, $\theta_{4a} = 5\deg$, $\theta_{4b} = 16\deg$, $\theta_{4c} = 42\deg$).

(a)   (b)

Figure 5. Simulation results of (a) the extracted external quality factor Q_e against L_{t1} (b) the extracted coupling coefficient k against s_1.

degree of the port excitation can be easily tuned by adjusting the proportion of θ_{3a} in θ_3 ($\theta_3 = \theta_{3a} + \theta_{3b}$). Calculated results are demonstrated in Fig. 4(b).

To further investigate the influences of physical dimensions on the port excitation and bandwidth, the extracted external quality factor Q_e and the coupling coefficient k are simulated based on the structures in Fig. 5(a) and Fig. 5(b), respectively. As demonstrated in Fig. 5, the quality factor Q_e is controlled by L_{t1} while the coupling coefficient k is determined by s_1.

2.2. Transmission Zeros

The TZs can be achieved by solving $S_{21} = 0$. Four TZs can be observed with two TZs located at the lower stopband, and the other two TZs located at the upper stopband. The location of the TZs is mainly controlled by the ETLs. The effects of θ_{4a} and K_2 $[K_2 = (Z_{e2}Z_{o2})/(Z_{e2} + Z_{o2})]$ on TZs are shown in Fig. 6(a) and Fig. 6(b), respectively. As can be seen from Fig. 6(a), TZ_1, TZ_3 and TZ_4 move to lower frequencies, while TZ_2 moves to higher frequencies when θ_{4a} increases. However, compared to TZ_1 and TZ_4, the changes of TZ_2 and TZ_3 are very small compared with their frequencies As demonstrated in Fig. 6(b), the locations of the TZs all change with K_2 distinctly TZ_1, TZ_2 and TZ_4 move to higher frequencies, while TZ_3 moves to lower frequencies when K_2 increases.
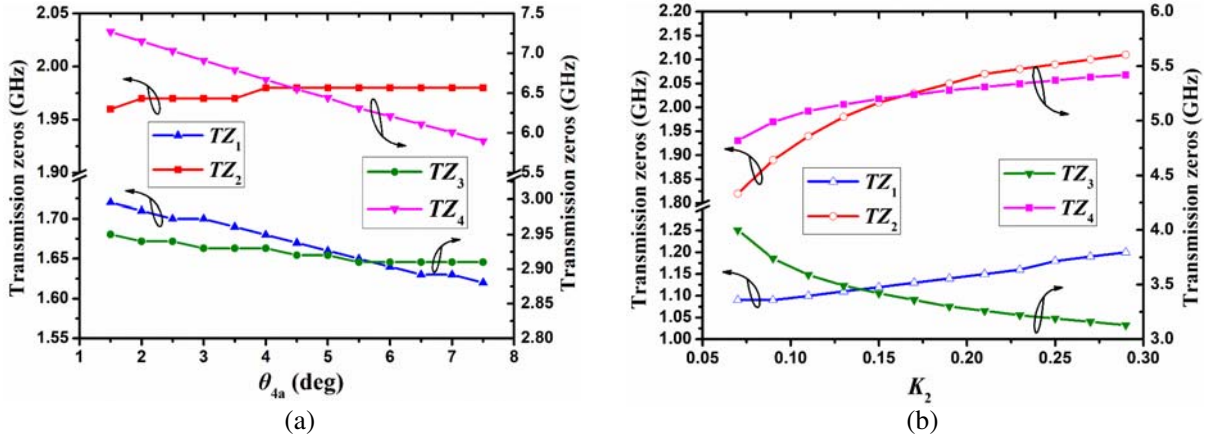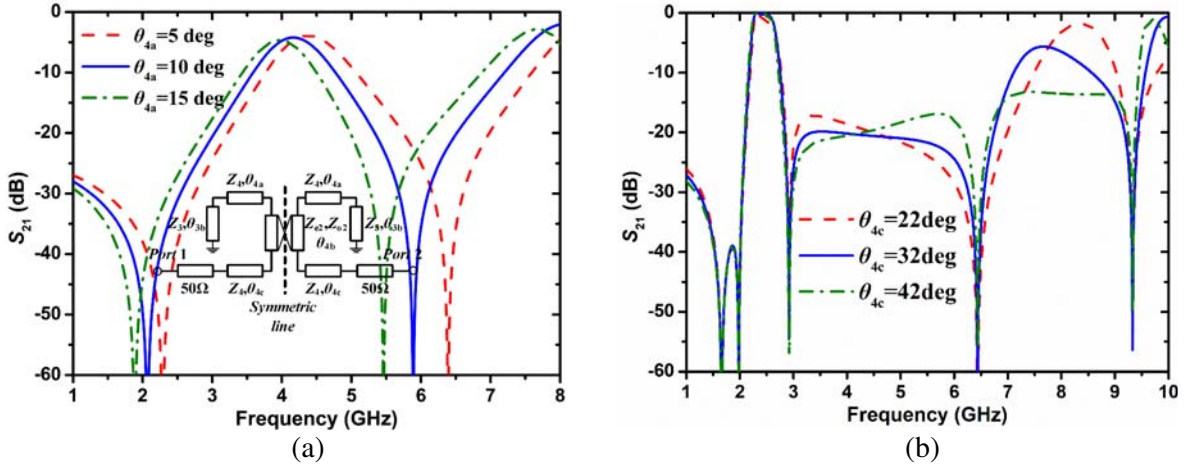

Figure 6. (a) Transmission zeros versus θ_{4a} ($Z_1 = 90\,\Omega$, $Z_{o1} = 32.3\,\Omega$, $Z_{e1} = 49.1\,\Omega$, $Z_3 = 94\,\Omega$, $Z_4 = 115\,\Omega$, $Z_{o2} = 79\,\Omega$, $Z_{e2} = 144.5\,\Omega$, $\theta_1 = 37\,\text{deg}$, $\theta_2 = 30\,\text{deg}$, $\theta_{3a} = 5\,\text{deg}$, $\theta_{3b} = 37.3\,\text{deg}$, $\theta_{4b} = 16\,\text{deg}$, $\theta_{4c} = 42\,\text{deg}$) (b) transmission zeros versus K_2 $[K_2 = (Z_{e2} - Z_{o2})/(Z_{e2} + Z_{o2})]$ ($Z_1 = 90\,\Omega$, $Z_{o1} = 32.3\,\Omega$, $Z_{e1} = 49.1\,\Omega$, $Z_3 = 94\,\Omega$, $Z_4 = 115\,\Omega$, $Z_{o2} = 40\,\Omega$, $\theta_1 = 37\,\text{deg}$, $\theta_2 = 30\,\text{deg}$, $\theta_{3a} = 5\,\text{deg}$, $\theta_{3b} = 37.3\,\text{deg}$, $\theta_{4b} = 16\,\text{deg}$, $\theta_{4c} = 42\,\text{deg}$).

In fact, the generation mechanisms of the TZs are different. Looking at the part in the green dotted frame in Fig. 1(b), the ETLs along with the shorted stub (Z_3, θ_{3b}) not only provide the source-load coupling, but also produce two extra TZs. The frequency responses of different θ_{4a} are plotted in Fig. 7(a). The changing trends of the two TZs in Fig. 7(a) are same to those of TZ_1 and TZ_4, when θ_{4a} increases.
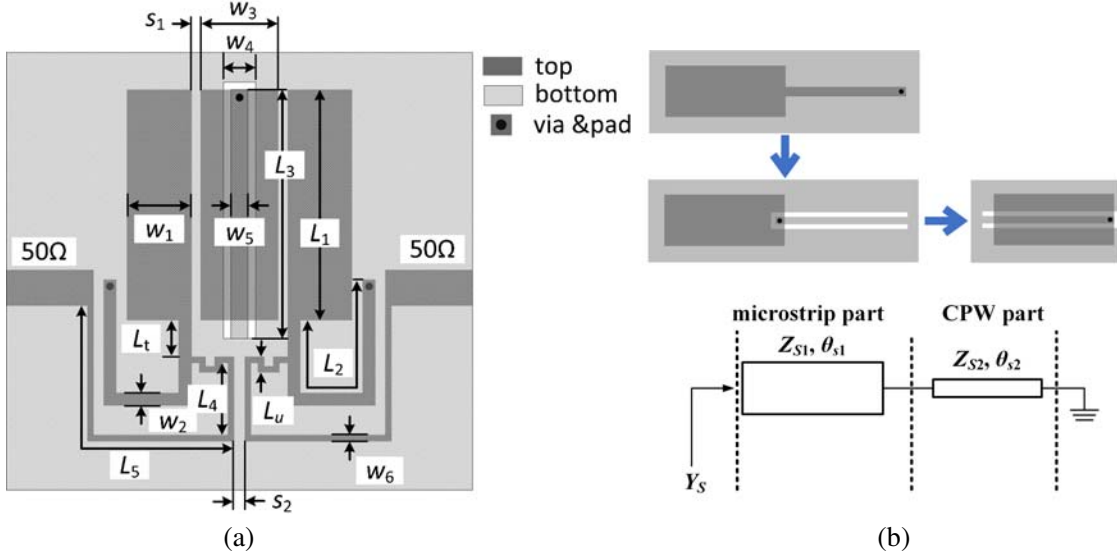
Above all, although the location of the TZs cannot be controlled individually, we can still arrange the distribution of the TZs by adjusting θ_{4a} and K_2. In addition, the extended part of the feeding line θ_{4a} is implemented to suppress the harmonic band of the proposed BPF. The calculated results are displayed in Fig. 7(b).

3. FULL WAVE SIMULATION AND MEASUREMENT

To validate our design methods, full-wave simulation is used. The physical configuration of the proposed BPF is displayed in Fig. 8(a). The second SIR is composed of a low Z microstrip section on the top

Figure 7. (a) The frequency responses of the ETLs with different θ_{4a} ($Z_1 = 90\,\Omega$, $Z_{o1} = 32.3\,\Omega$, $Z_{e1} = 49.1\,\Omega$, $Z_3 = 94\,\Omega$, $Z_4 = 115\,\Omega$, $Z_{o2} = 79\,\Omega$, $Z_{e2} = 144.5\,\Omega$, $\theta_1 = 37\deg$, $\theta_2 = 30\deg$, $\theta_{3a} = 5\deg$, $\theta_{3b} = 37.3\deg$, $\theta_{4b} = 16\deg$, $\theta_{4c} = 42\deg$) (b) the calculated frequency responses of different θ_{4c} ($Z_1 = 90\,\Omega$, $Z_{o1} = 32.3\,\Omega$, $Z_{e1} = 49.1\,\Omega$, $Z_3 = 94\,\Omega$, $Z_4 = 115\,\Omega$, $Z_{o2} = 79\,\Omega$, $Z_{e2} = 144.5\,\Omega$, $\theta_1 = 37\deg$, $\theta_2 = 30\deg$, $\theta_{3a} = 5\deg$, $\theta_{3b} = 37.3\deg$, $\theta_{4a} = 5\deg$, $\theta_{4b} = 16\deg$).


Figure 8. (a) Physical configuration. (b) Design process of the center SIR.

layer and a high Z CPW section on the ground plane connected by a metalized via with the radius of 0.15 mm. It is transformed from the traditional microstrip SIR by replacing the high impedance microstrip section with a CPW one and rotating the CPW section to the bottom of the microstrip one. The design process is shown in Fig. 8(b). The input admittance Y_s should be equal to zero under the resonant condition. Thus,

$$Y_s = \frac{Z_{s2}^2 - Z_{s1}Z_{s2}\tan\theta_{s1}\tan\theta_{s2}}{jZ_{s2}(Z_{s1}\tan\theta_{s1} + Z_{s2}\tan\theta_{s2})} = 0 \tag{11a}$$

$$Z_{s2}/Z_{s1} = \tan\theta_{s1}\tan\theta_{s2} \tag{11b}$$

Although the presence of the CPW part below affects the integrity of the microstrip structure slightly, we can still obtain the desired resonant frequency by adjusting the impedance and length of each part. This folded SIR is more miniaturized than traditional microstrip one. An experimental filter fabricated
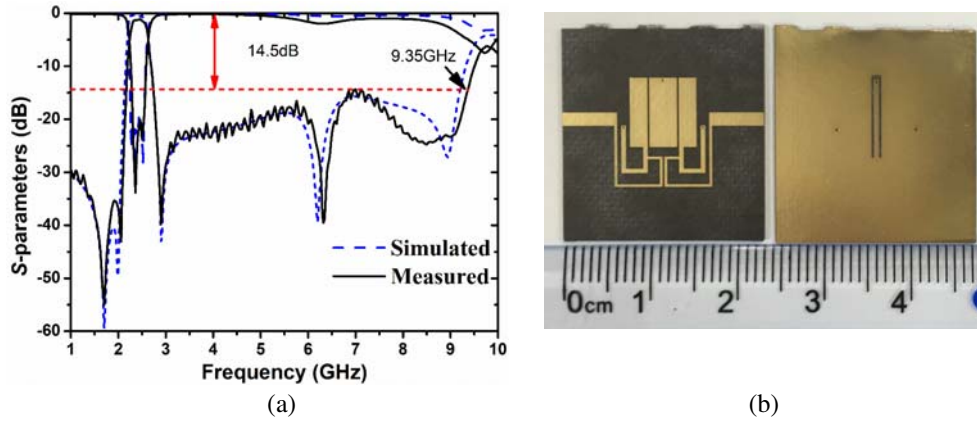
Figure 9. (a) Simulated and measured results of the proposed filter, (b) the pictures of the proposed BPF.

on Rogers RT/duroid 5880 ($\varepsilon_r = 2.2$, $\tan\delta = 0.0009$) with thickness of $0.508\,\mathrm{mm}$ is simulated and measured. The specific dimension parameters are as follows: $W_1 = 2$, $W_2 = 0.5$, $W_3 = 3.14$, $W_4 = 1.2$, $W_5 = 0.5$, $W_6 = 0.3$, $L_1 = 8$, $L_2 = 9.5$, $L_3 = 9.0$, $L_4 = 2.9$, $L_5 = 12.56$, $L_u = 0.3$, $L_t = 1.1$, $s_1 = 0.25$, $s_2 = 0.24$, units in mm.

The simulated and measured results are plotted in Fig. 9 for comparison. The measured passband is centered at $2.4\,\mathrm{GHz}$ with FBW of 8.3%. The measured minimum insertion is $1.12\,\mathrm{dB}$, with return loss better than $20\,\mathrm{dB}$. Four TZs are located at $1.70\,\mathrm{GHz}$, $2.06\,\mathrm{GHz}$, $2.90\,\mathrm{GHz}$ and $6.32\,\mathrm{GHz}$ respectively. The measured upper stopband is up to $9.35\,\mathrm{GHz}$ ($3.9f$) with rejection level of $14.5\,\mathrm{dB}$. Otherwise, the size of the filter is only $0.15\lambda_g * 0.13\lambda_g$, where λ_g is guide wavelength at f. The photograph of the fabricated BPF is plotted in Fig. 9(b). The comparison between the proposed filter and previous works is shown in Table 1. It is obvious that the proposed filter has the characteristics of high selectivity, wide stopband and compact size.

Table 1. Comparison between previous works and this work.

Refs	f_0 (GHz)	FBW (%)	Stopband	TZs	Size ($\lambda_g * \lambda_g$)
[3]	1.75	9.6	$20\,\mathrm{dB}$ at $4.6 * f_0$	4	$0.37 * 0.33$
[4]	2.0	3.65	N/A	2	$0.97 * 0.97$
[5]	1.0	5	N/A	2	$0.62 * 0.87$
[6]	2.0	8	$15\,\mathrm{dB}$ at $2.2 * f_0$	2	$0.35 * 0.33$
[9]	2.4	3.5	$30\,\mathrm{dB}$ at $2.3 * f_0$	3	$0.29 * 0.05$
This work	2.4	8.3	$14.5\,\mathrm{dB}$ at $3.9 * f_0$	4	$0.15 * 0.13$

4. CONCLUSION

A novel compact BPF using ETLs source-load coupling is designed, fabricated and measured. As the ETLs can provide the source-load coupling as well as two extra controllable TZs, the proposed filter can be designed with a great degree of freedom to realize high selectivity. Furthermore, a folded SIR of which the high Z section is realized by CPW on the ground plane is introduced. Thus, a high selectivity BPF in compact size is obtained. A filter sample is fabricated to validate the design method, and the measured results agree with the simulated ones well.

ACKNOWLEDGMENT

REFERENCES

1. Ding, J. Q., D. Liu, S. C. Shi, and W. Wu, "W-band quasi-elliptical waveguide filter with cross-coupling and source-load coupling," *Electronics Letters*, Vol. 52, No. 23, 1960–1961, 2016.

2. Wan, X. W. and M. Q. Li, "Tri-section stepped-impedance resonator filter with controllable mixed electric and magnetic cross-coupling," *Electronics Letters*, Vol. 53, No. 4, 255–256, 2017.

3. Wu, C. H., C. H. Wang, Y. S. Lin, and C. H. Chen, "Parallel-coupled coplanar-waveguide bandpass filter with multiple transmission zeros," *IEEE Microwave and Wireless Components Letters*, Vol. 17, No. 2, 118–120, 2007.

4. Zhang, X. C., Z. Y. Yu, and J. Xu, "Design of microstrip dual-mode filters based on source-load coupling," *IEEE Microwave and Wireless Components Letters*, Vol. 18, No. 10, 677–679, 2008.

5. Li, L. and Z. F. Li, "Application of inductive source-load coupling in microstrip dual-mode filter design," *Electronics Letters*, Vol. 46, No. 2, 141–142, 2010.

6. Dai, G. L., Y. X. Guo, and M. Y. Xia, "Design of compact bandpass filter with improved selectivity using source-load coupling," *Electronics Letters*, Vol. 46, No. 7, 505–506, 2010.

7. Xu, Z. Q., P. Wang, K. W. Qian, and Z. Tian, "Substrate integrated waveguide filter with embedded mixed source-load coupling," *Electronics Letters*, Vol. 49, No. 23, 1464–1465, 2013.

8. Xu, Z., Y. Shi, C. Xu C, P. Wang., "A novel dual mode substrate integrated waveguide filter with mixed source-load coupling (MSLC)," *Progress In Electromagnetics Research*, Vol. 136, 595–606, 2013.

9. Deng, H. W., F. Liu, T. Xu, L. Sun, and Y. F. Xue, "Compact and high selectivity dual-mode microstrip BPF with frequency-dependent source-load coupling," *Electronics Letters*, Vol. 54, No. 4, 219–221, 2018.

10. Li, L. and Z. Li, "Side-coupled shorted microstrip line for compact quasi-elliptic wideband bandpass filter design," *IEEE Microwave and Wireless Components Letters*, Vol. 20, No. 6, 322–324, 2010.

11. Zhu, L., S. Sun, and R. Li, *Microwave Bandpass Filters for Wideband Communications*, Chapters 2 and 3, 18–84, John Wiley & Sons. Inc., 2012.